AGU PUBLICATIONS

JGR

Journal of Geophysical Research: Oceans

RESEARCH ARTICLE

10.1002/2013JC009507

Usable solar radiation and its attenuation in the upper water column

Zhongping Lee[1], Shaoling Shang[2], Keping Du[3], Jianwei Wei[1], and Robert Arnone[4]

[1]School for the Environment, University of Massachusetts Boston, Boston, Massachusetts, USA, [2]State Key Laboratory of Marine Environmental Science, Xiamen University, Xiamen, China, [3]State Key Laboratory of Remote Sensing Science, School of Geography, Beijing Normal University, Beijing, China, [4]Department of Marine Science, University of Southern Mississippi, Stennis Space Center, Mississippi, USA

Key Points:
- A new radiometric term (USR) is defined
- Attenuation of USR is nearly constant vertically for oceanic waters
- USR and phytoplankton absorption speed the calculation of PUR

Correspondence to:
Z. Lee,
zhongping.lee@umb.edu

Citation:
Lee, Z., S. Shang, K. Du, J. Wei, R. Arnone (2014), Usable solar radiation and its attenuation in the upper water column, *J. Geophys. Res. Oceans*, *119*, doi:10.1002/2013JC009507.

Received 12 OCT 2013
Accepted 11 FEB 2014
Accepted article online 15 FEB 2014

Abstract A new radiometric term named as *usable solar radiation* (USR) is defined to represent the spectrally integrated solar irradiance in the spectral window of 400–560 nm. Through numerical simulations of optically deep waters covering a wide range of optical properties, it is found that the diffuse attenuation coefficient of downwelling USR, K_d(USR), is nearly a constant vertically for almost all oceanic waters (chlorophyll concentration under ~3 mg m^{-3}). This feature is quite contrary to the diffuse attenuation coefficient of the photosynthetic available radiation, K(PAR), which varies significantly from surface to deeper depths for oceanic waters. It is also found that the ratio of the photosynthetic utilizable radiation (PUR) to the product of USR and phytoplankton absorption coefficient at 440 nm approximates a constant for most oceanic waters. These results support the use of a single K_d(USR) for each water and each sun angle for accurate estimation of USR propagation, and suggest an efficient approach to estimate PUR(z) in the upper water column. These results further indicate that it is necessary and valuable for the generation of USR and K_d(USR) products from satellite ocean color measurements, which can be used to facilitate the studies of heat transfer and photosynthesis in the global oceans.

1. Introduction

Solar radiation is the driving force for biogeochemical processes on Earth. In the ocean, solar radiation drives photosynthesis and heating, as well as photo-oxidation of both dissolved and particulate matters [e.g., *Del Vecchio and Blough*, 2002; *Lewis et al*., 1990; *Platt and Sathyendranath*, 1988; *Zaneveld et al*., 1981]. Because most natural water bodies are not opaque, these processes happen not only at the ocean surface, but also at depth in the water column. To quantify the photosynthesis and heating in deeper waters, it is thus necessary to develop schemes to properly propagate surface solar radiation to deeper depths. Water molecules absorb strongly for wavelengths longer than 700 nm, and the solar radiation for wavelengths shorter than 400 nm is quite limited, so the penetration of solar radiation is primarily confined in the visible domain (400–700 nm) for global oceans. Generally, to ease the burden of calculating light field in large-scale studies and also to match a common light measurement in this visible domain, numerous studies implemented a simple expression for the propagation of visible radiation in the upper water column as [*Buiteveld*, 1995; *Kara et al*., 2005; *Murtugudde et al*., 2002; *Paulson and Simpson*, 1977]

$$PAR(z) = PAR(0^-) \times e^{-K(PAR)\times z}, \quad (1)$$

with PAR the photosynthetic available radiation (PAR, quanta m^{-2} s^{-1}) representing the total solar energy in the visible window (400–700 nm), and K(PAR) (m^{-1}) for the diffuse attenuation coefficient of PAR. Note that an equation of the same form is also commonly used for vertical penetration of broadband irradiance [*Mobley*, 1994; *Schofield et al*., 1999].

Therefore, for studies of the global oceans where the three-dimensional distribution of PAR(z) is required, it is necessary to know the spatial distributions of both PAR(0$^-$) and K(PAR), along with their temporal variations. To match this demand, at present PAR at sea surface and K(PAR) of the global oceans are routinely produced from ocean color satellites (http://oceancolor.gsfc.nasa.gov/cgi/l3). As a heritage product, the diffuse attenuation coefficient for spectral downwelling irradiance (E_d, W m^{-2} nm^{-1}) at 490 nm (K_d(490), m^{-1}) is also routinely produced. However, since K_d(490) is for a single wavelength, it cannot be applied directly for the propagation of PAR.

For the approach depicted by equation (1) to work properly, it requires K(PAR) to be a constant vertically. However, as discussed in many studies [e.g., *Morel*, 1988; *Smith et al*., 1989; *Lee*, 2009] and shown in *Zaneveld et al*. [1993], even for vertically homogeneous waters, due to the strong absorption by water molecules in the longer wavelengths (>600 nm), K(PAR) of oceanic waters is much larger in the surface layer and decreases significantly with depth [see e.g., *Lee*, 2009, Figure 1]. Thus, using a vertically constant K(PAR) value will result in significantly (a factor of 2 or more, depending on depth) incorrect PAR at depth, and consequently erroneous response of phytoplankton [*Penta et al*., 2008]. Note that there is a slight difference between the attenuation coefficient discussed in *Morel* [1988] and that in equation (1). The attenuation coefficient in *Morel* [1988] is for the downwelling part of the PAR property, while the PAR in equation (1) accounts for all photons from all directions with an equal weighting. But the upwelling PAR makes just about 5% of the total PAR, so the vertical attenuation nature of PAR is similar to that of the downwelling PAR.

To more properly account for visible radiation at depth, a better analytical approach is to use a spectral model for the propagation of solar radiation [*Morel*, 1988; *Sathyendranath and Platt*, 1988; *Simpson and Dickey*, 1981], with an expression such as

$$E_d(\lambda, z) = E_d(\lambda, 0^-) \times e^{-K_d(\lambda) \times z}. \quad (2)$$

Here $E_d(\lambda,z)$ is the downwelling spectral irradiance at depth z (m), with $K_d(\lambda)$ the spectral attenuation coefficient of $E_d(\lambda)$, and for wavelength λ (nm). For large-scale and long-term studies [e.g., *Gnanadesikan and Anderson*, 2009; *Murtugudde et al*., 2002; *Sweeney et al*., 2005], this approach will have a heavy computational load if the spectral resolution is set to very fine. It is thus always desirable to have an effective and at the same time reliable approach to propagate the visible radiation to depth, and various modifications of equation (1) have been developed in the past decades. For instance, *Morel and Antoine* [1994] found that it is feasible to use two exponential functions to describe this propagation for evaluating the feedback of phytoplankton on heating of the upper water column. The coefficients used for the two exponential functions are modeled as polynomial functions of chlorophyll concentration ([Chl], mg m^{-3}) [*Morel and Antoine*, 1994]. For the propagation of the full solar spectrum (250–2500 nm), *Ohlmann and Siegel* [2000] and *Ohlmann* [2003] also employed multiple exponential functions with model coefficients expressed as functions of [Chl]. In these approaches, there is no explicit separation of the spectral domain, so the spectral representation of each attenuation coefficient (or the so-called e-folding depth) is vague. In addition, since these approaches use [Chl] as input for the estimation of attenuation coefficient, they work best for Case-1 waters [*Morel*, 1988; *Morel and Prieur*, 1977] where all optical properties covary with [Chl]. However, as indicated in *Mobley et al*. [2004] and in *Lee and Hu* [2006], not all oceanic waters belong to Case-1 optically.

Because the attenuation coefficient is fundamentally determined by the inherent optical properties (IOPs) of the bulk water [*Kirk*, 1984; *Preisendorfer and Mobley*, 1984], *Lee et al*. [2005b] developed a two-component model to capture the vertical variation of the diffuse attenuation coefficient of downwelling irradiance in the visible domain—K_d(VIS), which uses IOPs and depth as inputs for its calculation. It is not possible to directly evaluate this K_d(VIS) product, however, unless there is a depth profile of K_d(VIS) from field measurements; although it could be done indirectly by comparing the modeled and measured PAR or solar radiation profiles [e.g., *Ohlmann*, 2003].

More recently, *Manizza et al*. [2005] and *Gnanadesikan and Anderson* [2009] explicitly divided the 400–700 nm range solar radiation into two wide spectral bands: the 400–560 nm range and the 560–700 nm range, and an attenuation coefficient was assigned specifically for each band. Values of these attenuation coefficients were considered as constants vertically and were further linked with [Chl] through a simple average of the spectral $K_d(\lambda)$ model developed by *Morel* [1988]. One advantage of this scheme is that the attenuation coefficient of each band has a clear spectral representation and can be adequately measured in the field, thus its characteristics and the model's robustness can be evaluated for all natural waters. However, the 400–560 nm spectral window is the most sensitive to changes of water constituents, as both phytoplankton and gelbstoff (or colored dissolved organic matter, CDOM) have their strongest optical signatures in this domain [e.g., *Mitchell*, 1990; *Sathyendranath and Platt*, 2007]. It is not yet known if the attenuation coefficient of this spectrally integrated radiation can be considered a constant vertically. It is thus necessary to characterize the nature of the attenuation coefficient of solar radiation in this wide spectral band.

Separately, because the average absorption coefficient in the 400–560 nm window is in general smaller than the average in the 400–700 nm window for most oceanic waters, light in the 400–560 nm window penetrates ~30% deeper than PAR [*Lee et al*., 2013]. Furthermore, light in this window contributes the most to photosynthesis [*Cullen et al*., 2012; *Morel*, 1978], it is thus useful to explore the potential of using radiation of this band for quick estimation of photosynthesis in global oceans. As with earlier studies [*Mobley et al*., 2002; *Morel and Gentili*, 2004; *Ohlmann*, 2003], we used numerical simulations to obtain adequate data sets of solar radiation in the 400–560 nm range, from which its vertical attenuation coefficient was calculated. We further characterized the vertical pattern of this attenuation and developed an analytical relationship that can be used for its quick estimation. Further, we evaluated the relationship between the photosynthetic utilizable radiation (PUR) and the solar radiation in this 400–560 nm window.

2. Definition of Usable Solar Radiation

Because photons in the 400–560 nm domain are the most abundant in the upper water column of oceanic waters and contribute the most to photosynthesis, we here define a radiometric term *usable solar radiation* (USR) to represent the spectrally integrated solar irradiance in this spectral window, and quantified as

$$USR_d(z) = \int_{400}^{560} E_d(z,\lambda)d\lambda. \tag{3}$$

Note that USR_d accounts for the downwelling portion of solar radiation and is measured in energy (units as W m^{-2}). Upwelling makes about 5% of the total radiation and can be estimated from the knowledge of water-leaving radiance measured by satellite sensors. Also, the energy can be easily converted to quanta if necessary [*Gordon and Morel*, 1983; *Morel and Smith*, 1974].

The above defined USR_d is conceptually different from the historically termed photosynthetic utilizable radiation (PUR) [*Cullen et al*., 2012; *Morel*, 1978]. For the downwelling component, which makes a majority of the total PUR, it can be written as

$$PUR_d(z) = \int_{400}^{700} E_d(z,\lambda) \times a_{ph}(z,\lambda)d\lambda, \tag{4}$$

with a_{ph} for phytoplankton absorption coefficient (m^{-1}). Here PUR_d, similarly as USR_d, is also measured in energy. Between USR_d and PUR_d, there are at least the following fundamental differences:

1. USR_d quantifies solar radiation in the blue-green domain that is *available and usable* for photosynthesis or water heating; while PUR_d quantifies solar radiation *absorbed already* by phytoplankton that can be used for photosynthesis [*Morel*, 1978];

2. The calculation of USR_d requires only information of E_d; while the calculation of PUR_d requires information of both E_d and a_{ph};

3. USR_d can be measured directly in the field with a radiometer; but PUR_d cannot be directly measured; and

4. With the measured vertical profiles of USR_d, its attenuation coefficient can also be easily calculated.

In addition, historical and current satellite ocean color sensors have more spectral bands placed in the 400–560 nm range [*IOCCG*, 1998], which makes it adequate for the estimation of USR from these measurements.

3. Numerical Simulations of USR_d

The diffuse attenuation coefficient for USR_d is defined as

$$\overline{K_d}(USR,z) = \frac{1}{z}\ln\left(\frac{USR_d(0^-)}{USR_d(z)}\right). \tag{5}$$

Note that this $\overline{K_d}(USR, z)$ represents an average value between sea surface and depth z, and that it is calculated from numerically simulated USR_d. As in numerous earlier studies [*Berwald et al*., 1995; *Cullen et al*., 2012; *Lee et al*., 1998a; *Mobley and Boss*, 2012; *Mobley et al*., 1993, 2002; *Morel and Loisel*, 1998], profiles of USR_d for various waters were simulated by Hydrolight (http://www.sequoiasci.com) [*Mobley and Sundman*, 2013]. In order to be consistent with earlier studies [*Lee et al*., 2005b, 2005c], we followed the same scheme for the simulation of downwelling spectral irradiance in the upper water column. Briefly, this simulated data set has the following features:

1. 500 spectral IOPs cover a spectral range of 400–700 nm with 10 nm spectral resolution [*IOCCG-OCAG*, 2003]; the absorption coefficient at 440 nm spans over a range of ~0.016–3.2 m^{-1}. There is no vertical variation of these IOPs (i.e., vertically uniform). In particular, these IOPs do not co-vary with chlorophyll concentration and encompass implicitly different phytoplankton functional types.

2. Input irradiance from the Sun and the sky is simulated with the *Gregg and Carder* [1990] model. Sun was positioned at 10°, 30°, and 60° from zenith, respectively, and the sky was set cloud free; with a wind speed of 5 m/s.

3. Information from bottom reflectance and inelastic scatterings (such as Raman scattering) were not considered (i.e., optically deep) since the focus of this study is oceanic waters, and the inelastic signal makes negligible contributions to total downwelling irradiance [*Morel and Gentili*, 2004], although can be quite strong relatively for the red-infrared spectral bands.

4. Ten geophysical depths (0, 1, 2, 4, 8, 20, 50, 100, 150, and 200 m) were designated for each Hydrolight run, which cover the entire euphotic zone.

4. Results and Discussion

4.1. Characteristics of K_d(USR)

From the above simulated profiles of $E_d(\lambda,z)$, $USR_d(z)$ was calculated following equation (3), which was then used for the calculation of $\overline{K_d}(USR, z)$ following equation (5). For each sun angle, 4500 $\overline{K_d}(USR, z)$ were calculated (9 $\overline{K_d}(USR, z)$ for each IOPs set). Figure 1a shows examples of the vertical variation of $\overline{K_d}(USR, z)$ for three different waters. It is found that generally $\overline{K_d}(USR, z)$ changes very mildly (<10%) with the increase of depth for these waters. For comparison, $\overline{K_d}(PAR, z)$ profiles of these waters were also calculated as in *Lee et al*. [2005b] and presented in Figure 1b. Clearly, $\overline{K_d}(PAR, z)$ shows significantly stronger vertical variation than $\overline{K_d}(USR, z)$. This contrast suggests that there is a possibility to use one attenuation value to describe the vertical attenuation coefficient $\overline{K_d}(USR, z)$, but it is not feasible to use one attenuation value for $\overline{K_d}(PAR, z)$ [*Morel*, 1988; *Smith et al*., 1989], at least for most oceanic waters.

To further characterize the vertical variability of $\overline{K_d}(USR, z)$, the coefficient of variation (CV) of $\overline{K_d}(USR, z)$, defined as the ratio of standard deviation to the mean, was calculated from the 9 $\overline{K_d}(USR, z)$ values for each IOPs set. Figure 2a shows the CVs of $\overline{K_d}(USR, z)$ for various waters (represented by K_d(490), and data of $K_d(490) < 0.5\ m^{-1}$ are shown). It is found that the CV of $\overline{K_d}(USR, z)$ is generally less than ~10%, while slightly >10% for K_d(490) between 0.2 and 0.3 m^{-1}. For the same waters, the CVs of $\overline{K_d}(PAR, z)$ were also calculated and shown in Figure 2b. The CVs of $\overline{K_d}(PAR, z)$ are generally between 10% and 50% for waters with $K_d(490) < 0.2\ m^{-1}$, and maintain around 5% for waters with $K_d(490) > 0.3\ m^{-1}$.

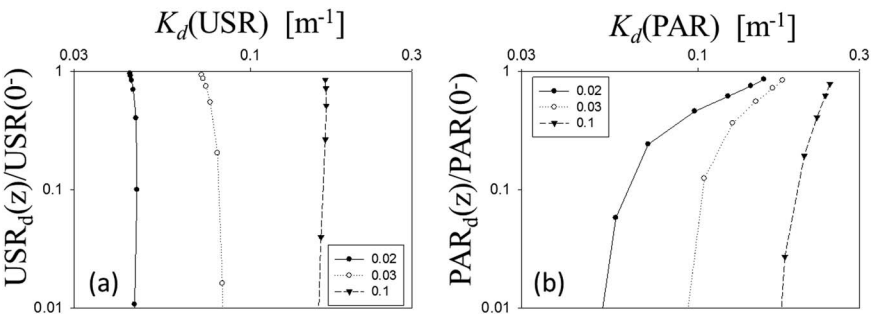

Figure 1. Examples of vertical variation of attenuation coefficient of spectrally integrated solar radiation, with Sun at 30° from zenith. (a) Attenuation of coefficient of USR and (b) Attenuation coefficient of PAR. Numbers in the box are absorption coefficient at 490 nm.

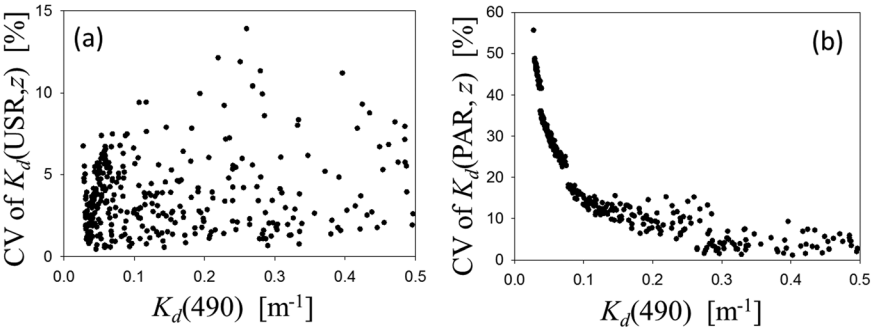

Figure 2. Coefficient of variation (CV) of vertically varying attenuation coefficient for waters with $K_d(490) < 0.5$ m^{-1}. (a) CV of K_d(USR, z) and (b) CV of K_d(PAR, z).

The vertical variation of $\overline{K_d}(USR,z)$ or $\overline{K_d}(PAR,z)$ is highly dependent on the spectral variation of $K_d(\lambda)$ for their respective spectral domains. For example, if $K_d(\lambda)$ is spectrally constant (such as a neutral filter), then there will be almost no change in vertical $\overline{K_d}(USR,z)$ or $\overline{K_d}(PAR,z)$. However, if $K_d(\lambda)$ changes significantly over wavelength, the spectral shape of $E_d(\lambda)$ will be quickly narrowed with the increase of depth [see examples in *Kishino et al*., 1984 and *Antoine et al*., 2013], then the attenuation of the spectrally integrated E_d (USR or PAR) will approach the value of the transparent window at deeper depths [*Smith et al*., 1989]. To help understand the CV contrast between $\overline{K_d}(USR,z)$ and $\overline{K_d}(PAR,z)$, Figure 3 shows a scatter plot between the ratio of max($K_d(\lambda)$) to min($K_d(\lambda)$) and K_d(490), but the ratio is calculated for either the USR spectral range (400–560 nm) or the PAR spectral range (400–700 nm), respectively. For the USR spectral range, the max($K_d(\lambda)$) to min($K_d(\lambda)$) ratio is within 2–4 for $K_d(490) < 0.5$ m^{-1}, but the ratio is as high as 25 (between ~4 and ~25 for $K_d(490) < 0.5$ m^{-1}) for the PAR spectral range. These features explain why for oceanic waters $\overline{K_d}(PAR,z)$ varies significantly with depth, while $\overline{K_d}(USR,z)$ is close to a constant. Also, for the 400–560 nm range, the max($K_d(\lambda)$) to min($K_d(\lambda)$) ratio is slightly higher for waters with K_d(490) between 0.2 and 0.3 m^{-1}, which explains a slightly higher $\overline{K_d}(USR,z)$ CV for these waters (see Figure 2a).

Note that from the MODIS-Aqua K_d(490) product for the global oceans and large lakes, there are ~98% of surface waters with K_d(490) less than 0.2 m^{-1} (equivalent [Chl] as ~3 mg m^{-3}). The above results thus suggest that for almost all global waters, it is adequate to use a vertically averaged $\overline{K_d}(USR)$ for a water body, instead of depth-dependent $\overline{K_d}(USR,z)$, to represent $\overline{K_d}(USR,z)$ for the calculation of USR_d in the upper water column. However, it is not appropriate to do the same for $\overline{K_d}(PAR,z)$ for oceanic waters, although the vertical variation of $\overline{K_d}(PAR,z)$ is much smaller for turbid waters (e.g., $K_d(490) > \sim 0.3$ m^{-1}, but under ~2.5 m^{-1}).

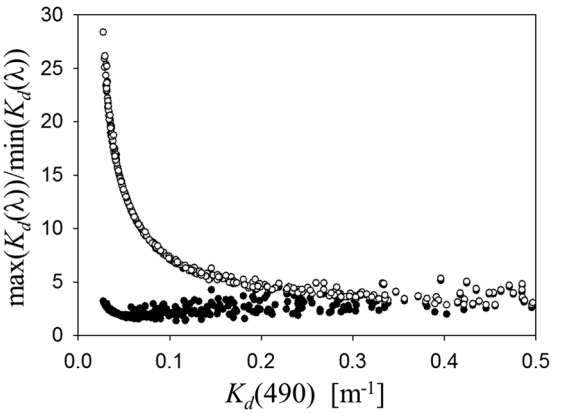

Figure 3. Scatter plot between K_d(490) and the ratio of maximum $K_d(\lambda)$ to minimum $K_d(\lambda)$ with λ in different ranges. Solid circle: ratio of $K_d(\lambda)$ for the USR spectral range; open circle: ratio of $K_d(\lambda)$ for the PAR spectral range.

4.2. Model of K_d(USR)

Since $\overline{K_d}(USR,z)$ can be considered as a constant vertically, the propagation of USR_d can then be expressed as

$$USR_d(z) = USR_d(0^-) \times e^{-K_d(USR) \times z}, \quad (6)$$

with K_d(USR) representing the vertically averaged $\overline{K_d}(USR,z)$. $USR_d(0^-)$ can be well estimated based on the Sun position and atmospheric properties; thus the estimation of $USR_d(z)$ of the global oceans depends on the determination of K_d(USR). Similar to earlier studies [*Morel et al*., 2007; *Zaneveld et al*., 1993], we here also use K_d(490) as the input for this estimation. This is based on two

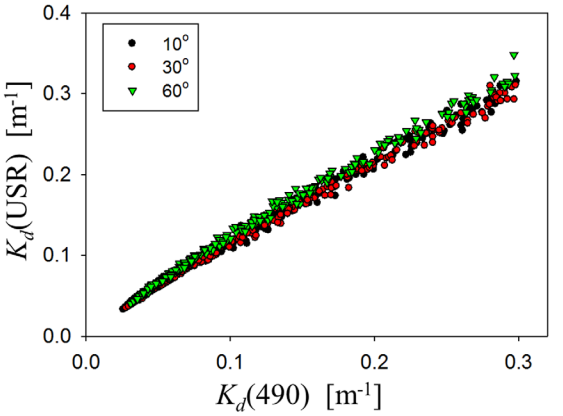

Figure 4. Relationship between K_d(USR) and K_d(490) of the three sun angles.

observations: (1) it is found that there is a strong correlation between K_d(USR) and K_d(490) (see Figure 4), and (2) K_d(490) are available from satellite ocean color remote sensing. For the numerically simulated data here and for K_d(490) less than 0.3 m^{-1}, the coefficient of determination (R^2) between K_d(USR) and K_d(490) is $>$ 0.99 for each sun angle. This is not surprising, given that the absorption coefficients of phytoplankton and gelbstoff are highly correlated spectrally and that 490 nm is roughly in the middle of the 400–560 nm range. From this observation, and following earlier approaches of modeling K_d(PAR) [*Morel et al*., 2007; *Zaneveld et al*., 1993], K_d(USR) is found can be well estimated from K_d(490), with

$$K_d(USR) \approx 0.94 K_d(490)^{0.90}. \quad (7)$$

The modeling coefficients (0.94 and 0.90) are averages for the three sun angles used in the simulations. The averaged absolute percentage difference between equation (7) modeled K_d(USR) and that of Hydrolight simulation is ~5%, suggesting highly reliable modeling results. K_d(USR) could also be estimated from K_d(440), but a slightly smaller coefficient of determination ($R^2 \sim 0.98$) was found.

To evaluate further the impact of this modeled K_d(USR) on the calculation of USR_d at depth, we compared equation (6)-modeled transmittance $Tr(z)$ ($= USR_d(z)/USR_d(0^-)$) with known (Hydrolight simulated) $Tr(z)$, but with K_d(USR) modeled using equation (7). In addition, the K_d(490) is modeled with the a and b_b values at 490 nm following the model of *Lee et al*. [2013], because K_d product could be better derived semianalytically from ocean color remote sensing [*Lee et al*., 2005a]. Figure 5a provides a scatter plot of the $Tr(z)$ between the analytically modeled (i.e., equation (6)) and Hydrolight-simulated values, with Figure 5b showing the histogram of the ratio of modeled $Tr(z)$ to known $Tr(z)$. Similarly as previously discussed, we limited the data to $K_d(490) < 0.2$ m^{-1} and data with $Tr(z) > 0.5\%$. For this restricted data set, but covering the entire euphotic zone and nearly all the oceanic waters, it is found that a significant majority (~90%) of this ratio is in a range of 0.9–1.1 (~95% for the ratio in a range of 0.8–1.2), indicating highly reliable modeled $Tr(z)$ with the above analytical approach, although using a single exponential function and a single K_d(USR) value for each water body and each sun angle. These results strongly support the scheme of using this simple and analytical system in general circulation models to study the contribution of biological pump on global carbon cycle as well as on heat transfer [*Gnanadesikan and Anderson*, 2009; *Jolliff et al*., 2012; *Takahashi et al*., 2002]. Further, with past and present satellite ocean color measurements, it is quite straightforward to generate the two USR products ($USR_d(0^-)$ and K_d(USR)) for the global oceans. Note that it is much easier to store and process

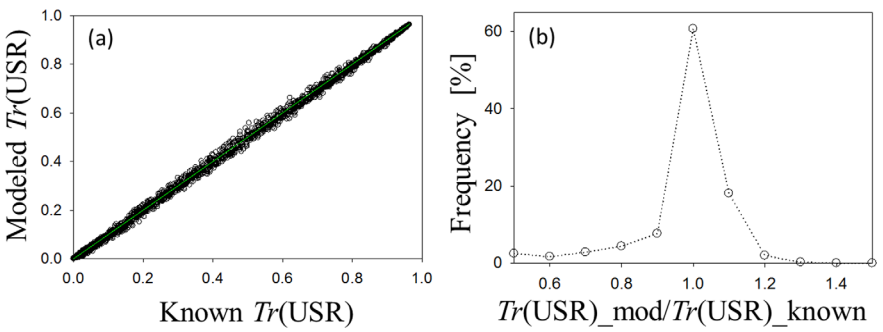

Figure 5. (a) Relationship between known USR transmittance (Tr(USR)) and modeled Tr(USR), green line is 1:1 and (b) Histogram of the ratio of modeled Tr(USR) to known Tr(USR).

satellite data with a smaller number of inputs or variables for large-scale studies. However, it is necessary to point out that K_d(USR) is not a simple arithmetic average of $K_d(\lambda)$ in the 400–560 nm range, although such a practice sometimes was used to model the wideband attenuation coefficients [e.g., *Manizza et al*., 2005].

Further, it is important to emphasize here that this K_d(USR) can be considered as a constant vertically, whereas the K_d(PAR) used in *Morel et al.* [2007] is specifically developed for the attenuation between the surface PAR and 1% of surface PAR, which cannot be used for other depth intervals, as K_d(PAR) is associated with significant vertical variation in the upper water column [*Morel*, 1988; *Smith et al*., 1989; *Zaneveld et al*., 1993]. In addition, the K_d(USR) model aims at optically deep, vertically homogeneous waters. For inhomogeneous waters, or for shallow waters where bottom reflectance makes a significant contribution to the water column irradiance, it requires more sophisticated schemes for the quantification of solar irradiance in the water column. One such approach is the recently developed EcoLight-S radiative transfer model [*Mobley*, 2011; *Mobley and Boss*, 2012], which can compute in-water spectral irradiances or PAR at any depth for given IOPs, bottom reflectance, or sky conditions.

4.3. Conversion of USR to PUR

One of the important mission goals of ocean color remote sensing is to estimate basin-scale primary production [*IOCCG*, 1998; *McClain*, 2009]. In addition to photo-physiological information, this process requires data of both light and phytoplankton for an accurate estimation [*Behrenfeld and Falkowski*, 1997; *Cullen*, 1990; *Marra et al*., 1992; *Sathyendranath et al*., 1989]. As discussed in *Morel* [1978], this estimation can be converted from PUR. To speed up the calculation of PUR at depth for the global oceans [*Cullen et al*., 2012], the following discusses the ratio of PUR_d to USR_d and its relationship to phytoplankton absorption coefficient. A quantity between PUR_d and USR_d is defined as

$$\gamma = \frac{PUR_d}{USR_d \times a_{ph}(440)}. \tag{8}$$

When this γ is known, USR_d can then be easily converted to PUR_d with known $a_{ph}(440)$. Note that the latter can be empirically or semianalytically derived from ocean color measurements [*IOCCG*, 2006; *Lee et al*., 1998b].

From the same numerically simulated data set, $PUR_d(z)$ is calculated following equation (4) for each IOPs set, with Figure 6 showing examples of $\gamma(z)$ for four different IOPs sets. It is interesting that although $a_{ph}(440)$ is varied by ~20 fold (the range of equivalent *Chl* is ~0.035–3 mg m^{-3}, ~85 fold), >80% of the γ values maintain in a range of 0.45–0.75 for $USR_d(z)$ within 1% of its surface value; and >70% of the γ values are within 0.5–0.7. To get a further characterization of γ, Figure 7a shows the distribution of γ from all simulations but limiting to $K_d(490) < 0.2$ m^{-1} ("clear" waters), and Figure 7b further limiting to $a_{ph}(440) < 0.1$ m^{-1} (equivalent [Chl] is ~ 3.0 mg m^{-3} based on the relationship in *Bricaud et al*. [1995]). From this further restricted data set, it is found that γ has an average value as 0.61 (mode as 0.62), and >82% is within a range of 0.5–0.7. These results indicate that PUR in the upper water column of "clear" waters can be well (with an uncertainty of ~±14%) expressed as

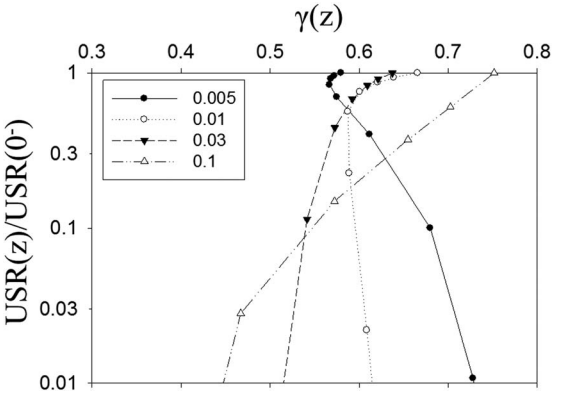

Figure 6. Examples of vertical profile of $\gamma(z)$. Values in the box for $a_{ph}(440)$ value.

$$PUR_d \approx 0.61 USR_d \times a_{ph}(440). \tag{9}$$

This simple relationship, although not 100% accurate, significantly reduces the complexity in calculating absorbed energy in the upper water column for photosynthesis of the global oceans [*Cullen et al*., 2012; *Lehmann et al*., 2004], as both $a_{ph}(440)$ and $USR_d(z)$ can be handily derived from satellite ocean color measurements. The uncertainty

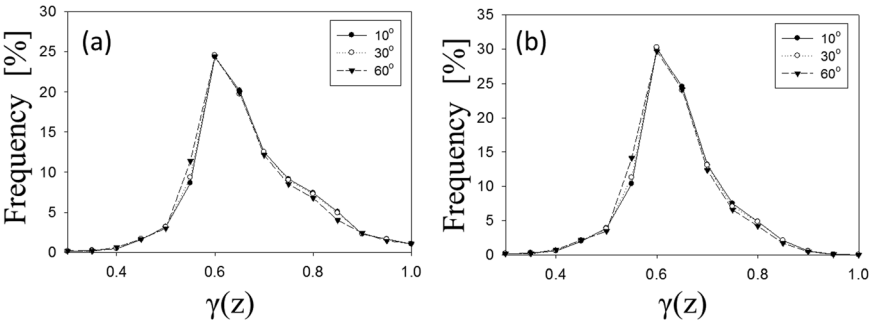

Figure 7. Distribution of $\gamma(z)$ for three sun angles: (a) for data with USR(z)/USR(0) > 1% and (b) for data with USR(z)/USR(0) > 1% and $a_{ph}(440) \leq 0.1\ m^{-1}$.

will be higher for deeper waters (where USR_d is smaller than 1% of surface value), but its contribution to water-column primary productivity is significantly limited due to the very small (<1%) USR_d values in these depths, thus rendering this higher uncertainty of estimated $PUR_d(z)$ in deeper waters tolerable.

5. Conclusions

From numerically simulated downwelling USR (USR_d) profiles of oceanic waters covering a wide range of water properties, it is found that for "clear" waters ($K_d(490) < 0.2\ m^{-1}$), the attenuation coefficient of USR_d ($\overline{K_d}(USR, z)$) is nearly a constant vertically. In contrast, the attenuation coefficient of PAR can differ vertically by a factor for 4 for such waters. This feature of $\overline{K_d}(USR, z)$ supports the practice of calculating USR_d in the upper water column with two simple inputs: $USR_d(0^-)$ and K_d(USR)—an average of $\overline{K_d}(USR, z)$ in the upper water column. Note that >98% of the global oceans are with $K_d(490) < 0.2\ m^{-1}$.

Separately, it is found that the ratio of $PUR_d(z)$ to ($USR_d(z) \times a_{ph}(440)$) has an average as 0.61 for "clear" waters, and >80% are within a range of 0.5–0.7. Such a finding makes it easy and feasible for the estimation of $PUR_d(z)$ without involving full-spectral calculations for about 98% of the global oceans. These results significantly alleviate the computational burden of large-scale studies while at the same time maintaining reasonable reliability (within ~14% uncertainty). These features, along with the capacity of ocean-color satellite sensors, make it not only valuable, but also practical, to generate USR products ($USR_d(0^-)$ and K_d(USR)) from ocean color measurements for studies of biogeochemical processes and heat transfer in the global oceans. However, the above results are based solely on numerical simulations; it is important and necessary to validate such findings with adequate data from field measurements.

Acknowledgments
We are grateful for the financial support from the University of Massachusetts Boston, NASA Ocean Biology and Biogeochemistry and Water and Energy Cycle Programs and the JPSS VIIRS Ocean Color Cal/Val Project, from the National Natural Science Foundation of China (41071223, Du; 40976068 and 41121091, Shang) and Ministry of Science and Technology of China (2013BAB04B00, Shang).

References

Antoine, D., S. B. Hooker, S. Bélanger, A. Matsuoka, and M. Babin (2013), Apparent optical properties of the Canadian Beaufort Sea: Part 1: Observational overview and water column relationships, *Biogeosciences*, *10*, 4493–4509.

Behrenfeld, M. J., and P. G. Falkowski (1997), A consumer's guide to phytoplankton primary productivity models, *Limnol. Oceanogr.*, *42*, 1479–1491.

Berwald, J., D. Stramski, C. D. Mobley, and D. A. Kiefer (1995), Influences of absorption and scattering on vertical changes in the average cosine of the underwater light field, *Limnol. Oceanogr.*, *40*, 1347–1357.

Bricaud, A., M. Babin, A. Morel, and H. Claustre (1995), Variability in the chlorophyll-specific absorption coefficients of natural phytoplankton: Analysis and parameterization, *J. Geophys. Res.*, *100*, 13,321–13,332.

Buiteveld, H. (1995), A model for calculation of diffuse light attenuation (PAR) and Secchi depth, *Neth. J. Aquat. Ecol.*, *29*, 55–65.

Cullen, J. J. (1990), On models of growth and photosynthesis in phytoplankton, *Deep Sea Res., Part A*, *37*, 667–683.

Cullen, J. J., R. F. Davis, and Y. Huot (2012), Spectral model of depth-integrated water column photosynthesis and its inhibition by ultraviolet radiation, *Global Biogeochem. Cycles*, *26*, GB1011, doi:10.1029/2010GB003914.

Del Vecchio, R., and N. V. Blough (2002), Photobleaching of chromophoric dissolved organic matter in natural waters: Kinetics and modeling, *Mar. Chem.*, *78*, 231–253.

Gnanadesikan, A., and W. G. Anderson (2009), Ocean water clarity and the ocean general circulation in a coupled climate model, *J. Phys. Oceanogr.*, *39*, 314–332.

Gordon, H. R., and A. Morel (1983), *Remote Assessment of Ocean Color for Interpretation of Satellite Visible Imagery: A Review*, 44 pp., Springer, New York.

Gregg, W. W., and K. L. Carder (1990), A simple spectral solar irradiance model for cloudless maritime atmospheres, *Limnol. Oceanogr.*, *35*, 1657–1675.

IOCCG (1998), Minimum requirements for an operational ocean-color sensor for the open ocean, in *Reports of the International Ocean-Color Coordinating Group, No. 1*, edited by A. Morel, Halifax, Canada.

IOCCG (2006), Remote sensing of inherent optical properties: Fundamentals, tests of algorithms, and applications, in *Reports of the International Ocean-Colour Coordinating Group, No. 5*, edited by Z.-P. Lee, p. 126, Dartmouth, Canada.
IOCCG-OCAG (2003), Model, parameters, and approaches that used to generate wide range of absorption and backscattering spectra, Dartmouth, Canada. [Available at http://www.ioccg.org/groups/OCAG_data.html.]
Jolliff, J. K., T. A. Smith, C. N. Barron, S. deRada, S. C. Anderson, R. W. Gould, and R. A. Arnone (2012), The impact of coastal phytoplankton blooms on ocean-atmosphere thermal energy exchange: Evidence from a two-way coupled numerical modeling system, *Geophys. Res. Lett.*, *39*, L24607, doi:10.1029/2012GL053634.
Kara, A. B., A. J. Wallcraft, and H. E. Hurlburt (2005), Sea surface temperature sensitivity to water turbidity from simulations of the turbid Black Sea using HYCOM, *J. Phys. Oceanogr.*, *35*, 33–54.
Kirk, J. T. O. (1984), Dependence of relationship between inherent and apparent optical properties of water on solar altitude, *Limnol. Oceanogr.*, *29*, 350–356.
Kishino, M., C. R. Booth, and N. Okami (1984), Underwater radiant energy absorbed by phytoplankton, detritus, dissolved organic matter, and pure water, *Limnol. Oceanogr.*, *29*, 340–349.
Lee, Z. (2009), KPAR: An optical property associated with ambiguous values, *J. Lake Sci*, *21*, 159–164.
Lee, Z., C. Hu, S. Shang, K. Du, M. Lewis, R. Arnone, and R. Brewin (2013), Penetration of UV-Visible solar light in the global oceans: Insights from ocean color remote sensing, *J. Geophys. Res.*, *118*, 4241–4255, doi:10.1002/jgrc.20308.
Lee, Z. P., and C. Hu (2006), Global distribution of Case-1 waters: An analysis from SeaWiFS measurements, *Remote Sens. Environ.*, *101*, 270–276.
Lee, Z. P., K. L. Carder, C. D. Mobley, R. G. Steward, and J. S. Patch (1998a), Hyperspectral remote sensing for shallow waters: 1: A semianalytical model, *Appl. Opt.*, *37*, 6329–6338.
Lee, Z. P., K. L. Carder, R. G. Steward, T. G. Peacock, C. O. Davis, and J. S. Patch (1998b), An empirical algorithm for light absorption by ocean water based on color, *J. Geophys. Res.*, *103*, 27,967–27,978.
Lee, Z. P., M. Darecki, K. L. Carder, C. Davis, D. Stramski, and W. J. Rhea (2005a), Diffuse attenuation coefficient of downwelling irradiance: An evaluation of remote sensing methods, *J. Geophys. Res.*, *110*, C02017, doi:10.1029/2004JC002573.
Lee, Z. P., K. Du, R. Arnone, S. C. Liew, and B. Penta (2005b), Penetration of solar radiation in the upper ocean: A numerical model for oceanic and coastal waters, *J. Geophys. Res.*, *110*, C09019, doi:10.1029/2004JC002780.
Lee, Z. P., K. P. Du, and R. Arnone (2005c), A model for the diffuse attenuation coefficient of downwelling irradiance, *J. Geophys. Res.*, *110*, C02016, doi:10.1029/2004JC002275.
Lehmann, M. K., R. F. Davis, Y. Huot, and J. J. Cullen (2004), Spectrally weighted transparency in models of water-column photosynthesis and photoinhibition by ultraviolet radiation, *Mar. Ecol. Prog. Ser.*, *269*, 101–110.
Lewis, M. R., M. Carr, G. Feldman, W. Esaias, and C. McMclain (1990), Influence of Penetrating solar radiation on the heat budget of the equatorial pacific ocean, *Nature*, *347*, 543–545.
Manizza, M., C. L. Quere, A. J. Watson, and E. T. Buitenhuis (2005), Bio-optical feedbacks among phytoplankton, upper ocean physics and sea ice in a global model, *Geophys. Res. Lett.*, *32*, L05603, doi:10.1029/2004GL020778.
Marra, J., et al. (1992), Estimation of seasonal primary production from moored optical sensors in the Sargasso Sea, *Deep Sea Res.*, *97*, 7399–7412.
McClain, C. R. (2009), A decade of satellite ocean color observations, *Annu. Rev. Mar. Sci.*, *1*, 19–42.
Mitchell, B. G. (1990), Algorithms for determining the absorption coefficient for aquatic particles using the quantitative filter technique, *Proc. SPIE, 1302*, doi:10.1117/12.21440.
Mobley, C. D. (1994), *Light and Water: Radiative Transfer in Natural Waters*, pp. 265–285, Academic, New York.
Mobley, C. D. (2011), Fast light calculations for ocean ecosystem and inverse models, *Opt. Express*, *19*, 18,927–18,944.
Mobley, C. D., and E. S. Boss (2012), Improved irradiances for use in ocean heating, primary production, and photo-oxidation calculations, *Appl. Opt.*, *51*, 6549–6560.
Mobley, C. D., and L. K. Sundman (2013), *HydroLight 5.2 User's Guide*, Sequoia Sci. Inc., Bellevue, Wash.
Mobley, C. D., B. Gentili, H. R. Gordon, Z. Jin, G. W. Kattawar, A. Morel, P. Reinersman, K. Stamnes, and R. H. Stavn (1993), Comparison of numerical models for computing underwater light fields, *Appl. Opt.*, *32*, 7484–7504.
Mobley, C. D., L. K. Sundman, and E. Boss (2002), Phase function effects on oceanic light fields, *Appl. Opt.*, *41*, 1035–1050.
Mobley, C. D., D. Stramski, W. P. Bissett, and E. Boss (2004), Optical modeling of ocean waters: Is the Case 1–Case 2 classification still useful?, *Oceanography*, *17*, 60–67.
Morel, A. (1978), Available, usable, and stored radiant energy in relation to marine photosynthesis, *Deep Sea Res.*, *25*, 673–688.
Morel, A. (1988), Optical modeling of the upper ocean in relation to its biogenous matter content (Case I waters), *J. Geophys. Res.*, *93*, 10,749–10,768.
Morel, A., and D. Antoine (1994), Heating rate within the upper ocean in relation to its bio-optical state, *J. Phys. Oceanogr.*, *24*, 1652–1665.
Morel, A., and B. Gentili (2004), Radiation transport within oceanic (case 1) water, *J. Geophys. Res.*, *109*, C06008, doi:10.1029/2003JC002259.
Morel, A., and H. Loisel (1998), Apparent optical properties of oceanic water: Dependence on the molecular scattering contribution, *Appl. Opt.*, *37*, 4765–4776.
Morel, A., and L. Prieur (1977), Analysis of variations in ocean color, *Limnol. Oceanogr.*, *22*, 709–722.
Morel, A., and R. C. Smith (1974), Relation between total quanta and total energy for aquatic photosynthesis, *Limnol. Oceanogr.*, *19*, 591–600.
Morel, A., H. Claustre, D. Antoine, and B. Gentili (2007), Natural variability of bio-optical properties in Case 1 waters: Attenuation and reflectance within the visible and near-UV spectral domains, as observed in South Pacific and Mediterranean waters, *Biogeosciences*, *4*, 913–925.
Murtugudde, R., J. Beauchamp, C. R. McClain, M. Lewis, and A. J. Busalacchi (2002), Effects of penetrative radiation on the upper tropical ocean circulation, *J. Clim.*, *15*, 470–486.
Ohlmann, J. C. (2003), Ocean radiant heating in climate models, *J. Clim.*, *16*, 1337–1351.
Ohlmann, J. C., and D. Siegel (2000), Ocean radiant heating: Part II: Parameterizing solar radiation transmission through the upper ocean, *J. Phys. Oceanogr.*, *30*, 1849–1865.
Paulson, C. A., and J. J. Simpson (1977), Irradiance measurements in the upper ocean, *J. Phys. Oceanogr.*, *7*, 953–956.
Penta, B., Z. Lee, R. M. Kudela, S. L. Palacios, D. J. Gray, J. K. Jolliff, and I. G. Shulman (2008), An underwater light attenuation scheme for marine ecosystem models, *Opt. Express*, *16*, 16,581–16,591.
Platt, T., and S. Sathyendranath (1988), Oceanic primary production: Estimation by remote sensing at local and regional scales, *Science*, *241*, 1613–1620.

Preisendorfer, R. W., and C. D. Mobley (1984), Direct and inverse irradiance models in hydrologic optics, *Limnol. Oceanogr.*, *29*, 903–929.
Sathyendranath, S., and T. Platt (1988), The spectral irradiance field at the surface and in the interior of the ocean: A model for applications in oceanography and remote sensing, *J. Geophys. Res.*, *93*, 9270–9280.
Sathyendranath, S., and T. Platt (2007), Spectral effects in bio-optical control on the ocean system, *Oceanologia*, *49*, 5–39.
Sathyendranath, S., T. Platt, C. M. Caverhill, R. E. Warnock, and M. R. Lewis (1989), Remote sensing of oceanic primary production: Computations using a spectral model, *Deep Sea Res.*, *36*, 431–453.
Schofield, O., J. Grzymski, W. P. Bissett, G. J. Kirkpatrick, D. F. Millie, M. Moline, and C. S. Roesler (1999), Optical monitoring and forecasting systems for harmful algal blooms: Possibility or pipe dream?, *J. Phycol.*, *35*, 1477–1496.
Simpson, J. J., and T. D. Dickey (1981), Alternative parameterizations of downward irradiance and their dynamic significance, *J. Phys. Oceanogr.*, *11*, 876–882.
Smith, R. C., J. Marra, M. J. Perry, K. S. Baker, E. Swift, E. Buskey, and D. A. Kiefer (1989), Estimation of a photon budget for the upper ocean in the Sargasso Sea, *Limnol. Oceanogr.*, *34*, 1673–1693.
Sweeney, C., A. Gnanadesikan, S. M. Griffies, M. J. Harrison, A. J. Rosati, and B. L. Samuels (2005), Impacts of shortwave penetration depth on large-scale ocean circulation and heat transport, *J. Phys. Oceanogr.*, *35*, 1103–1119.
Takahashi, M., S. C. Sutherland, and C. Sweeney (2002), Global sea-air CO_2 flux based on climatological surface ocean pCO2, and seasonal biological and temperature effects, *Deep Sea Res., Part II*, *49*(9–10), 1601–1622.
Zaneveld, J. R. V., J. C. Kitchen, and H. Pak (1981), The influence of optical water type on the heating rate of a constant depth mixed layer, *J. Geophys. Res.*, *86*, 6426–6428.
Zaneveld, J. R. V., J. C. Kitchen, and J. L. Mueller (1993), Vertical structure of productivity and its vertical integration as derived from remotely sensed observations, *Limnol. Oceanogr.*, *38*, 1384–1393.